JPEDAV (2016) 37:718–725
DOI: 10.1007/s11669-016-0502-y
1547-7037 ©ASM International

Isothermal Section of the Al-Mn-Dy System at 500 °C

Jie-li Meng, Jian-lie Liang, Jin-ming Zhu, and Kai-zhen Li

(Submitted December 16, 2015; in revised form September 2, 2016; published online October 21, 2016)

Phase relationships in the Al-Mn-Dy ternary system at 500 °C have been investigated by X-ray diffraction, scanning electron microscopy with energy dispersive spectroscopy, and electron probe microanalysis. From the experimental results it was concluded that the isothermal section consists of 16 single-phase regions, 26 two-phase regions and 12 three-phase regions. Two extensive solid solutions, $(Al_xMn_{1-x})_{12}Dy$ and $(Al_{1-x}Mn_x)_2Dy$, were observed. The solid solution $(Al_xMn_{1-x})_{12}Dy$ forms by Al replacing Mn in $Mn_{12}Dy$, while the continuous solid solution $(Al_{1-x}Mn_x)_2Dy$ forms by Mn and Al mutually substituting in Al_2Dy and Mn_2Dy, respectively. The maximum solid solubility of Al in $Mn_{12}Dy$ is 79.3 at.%.

Keywords Al-Mn-Dy alloy, phase diagram, x-ray diffraction

1. Introduction

Phase diagrams and thermodynamics provide basic knowledge for alloy design. For example, thermodynamic descriptions of multi-component Al-based alloys have been applied to alloy development.[1] Rare earth (RE) elements and transition metals play important roles in the improvement of the microstructure as well as the mechanical properties of Al-based alloys. Scandium was reported to greatly improve the properties of Al alloys due to the formation of coherent Al_3Sc.[2,3] The presence of Al_3Dy was observed to significantly reduce the microelectronic resistivity of the Al-Dy alloy thin films.[4]

A major alloying element in 3000 series commercial Al alloys is Mn. Work on the interaction of RE metals with transition metals and aluminum has been reported.[5-11] However, little work on phase equilibria of RE metals, manganese and aluminum was found in the open literature. In order to clarify the interaction of Mn and RE metals in commercial aluminum alloys, it is necessary to investigate phase equilibria in the Al-Mn-RE ternary system. Specifically, this work aims to investigate the phase equilibria in the Al-Mn-Dy system.

Five intermetallic compounds have been reported in the Al-Dy system[12] at 500 °C, i.e. Al_3Dy (rhombohedral Al_3Ho type), Al_2Dy (cubic Cu_2Mg type), AlDy (orthorhombic AlEr type), Al_2Dy_3 (tetragonal Al_2Zr_3 type) and $AlDy_2$ (orthorhombic Co_2Si type); three intermediate phases have been reported in the Mn-Dy system,[13] i.e., Mn_2Dy (cubic Cu_2Mg type), $Mn_{23}Dy_6$ (cubic $Mn_{23}Th$ type) and $Mn_{12}Dy$ (tetragonal $Mn_{12}Th$ type); and six intermetallic compounds have been reported in the Al-Mn system, i.e.$Al_{12}Mn$ (cubic $Al_{12}W$ type), Al_6Mn (orthorhombic Al_6Mn type), λ-Al_4Mn, μ-Al_4Mn, $Al_{11}Mn_4$ (triclinic $Al_{11}Mn_4$ type), and Al_8Mn_5 (rhombohedral Al_8Cr_5 type).[14,15] The λ-Al_4Mn and μ-Al_4Mn phases are compositionally and structurally different. For example, λ-Al_4Mn is in the Al-rich side with space group $P6_3/mmc$, while μ-Al_4Mn is in the Al-poor side with space group Pnnn. With temperature decreasing, $Al_{11}Mn_4$ transforms from the high temperature structure (Space group Pnma) to the low temperature form (space group $P\bar{1}$) at 916 °C. Table 1 lists crystallographic data of compounds stable at 500 °C in Al-Mn-Dy and one can see that there are no ternary compounds in this system.

Jie-li Meng, Jian-lie Liang, Jin-ming Zhu, and **Kai-zhen Li,** School of Science, Guangxi University for Nationalities, Nanning 530006, Guangxi, China. Contact e-mail: jieli_meng@126.com.

2. Experimental Procedure

The starting materials were high purity Al (99.95%), Mn (99.8%) and Dy (99.95%) (in mass%) and the total weight of each sample was 1.5 g. Specimens were melted in an arc furnace under an environment of pure Ar (99.99%). To compensate for the loss of Mn, an additional 20 wt.% Mn was added to each alloy. To guarantee homogeneity, the alloy buttons were melted at least three times. The final measured compositions were observed to slightly deviate from the nominal or synthesis composition of alloy, which shows that the loss of Mn in the alloy is compensated by the above mentioned method. After melting, the buttons were sealed in vacuum quartz tubes and then annealed at 500 °C for 30 days. The tubes were quenched into water after annealing, and then broken to recover the samples. The quenched alloys were cut into two pieces, one for x-ray examination and the other for microscopic analysis. The x-ray diffraction radiation was $Cu_{K\alpha}$.

Samples for x-ray diffraction were directly ground into powder, while samples for microstructure analysis were prepared by grinding and polishing. The microstructure of unetched samples was observed on the Zeiss EVO-18 scanning electronic microscope (SEM) equipped with energy dispersive spectroscopy (EDS). Some samples were analyzed using the JEOL JXA-8230 electron probe microanalyzer (EPMA), as well. Reported compositions are the average of three measurements.

Table 1 Crystallographic data of the compounds in Al-Mn-Dy system

Phases	Space group	Pearson symbol	Prototype	Lattice parameter (nm)			References
				a	b	c	
Al	Fm-3m	cF4	Cu	0.4049			16
Mn	$P4_132$	Cp20	βMn	0.629			17
	I-43m	cI58	αMn	0.8894			18
Dy	$P6_3/mmc$	Hp2	Mg	0.3458		0.5466	19
Al_3Dy	R-3m	hR20	Al_3Ho	0.608		3.594	20,21
	P63/mmc	hP16	Ni_3Ti	0.6091		0.9533	22
Al_2Dy	Fd-3m	cF24	Cu_2Mg	0.7843			23
AlDy	Pbcm	oP16	AlDy	0.5822	1.1369	0.5604	24
	Pm-3m	cP2	ClCs	0.3682			25
Al_2Dy_3	$P4_2nm$	tP20	Al_2Gd_3	0.8170		0.7523	26
	$P4_2mnm$	tP20	Al_2Zr_3	0.8218		0.755	27
$AlDy_2$	Pnma	oP12	Co_2Si	0.6543	0.5075	0.9397	28
$Mn_{12}Dy$	I4/mmm	tI26	$Mn_{12}Th$	0.8579		0.4763	29
$Mn_{23}Dy_6$	Fm-3m	Cf116	$Mn_{23}Th_6$	1.2358			30
Mn_2Dy	Fd-3m	cF24	Cu_2Mg	0.7564			31
$Al_{12}Mn$	Im-3m	cI26	$Al_{12}W$	0.747			32
Al_6Mn	Cmcm	oC28	Al_6Mn	0.7551	0.6497	0.8870	33
	Cmcm	oC28	Al_6Mn	0.7555	0.6499	0.8872	34
$Al_4Mn(\mu)$	Pnnn	oP60		0.7217	0.7674	0.875	35
$Al_4Mn(\lambda)$	P63/mmc	hP574	Al_4Mn	1.998(1)		2.4673	36
$Al_{11}Mn_4$	P-1	aP15	$Al_{11}Mn_4$	0.5095	0.8879	0.5051	37
Al_8Mn_5	R3m	hR52	Al_8Cr_5	1.2645		1.5855	38
AlMnDy	Fd-3m	cF-24	Cu_2Mg	0.778			31
Al_7Mn_5Dy	I4/mmm	tI26	$Mn_{12}Th$	0.8812		0.5096	39
Al_6Mn_6Dy	I4/mmm	tI26	$Mn_{12}Th$	0.8823		0.5061	39
Al_8Mn_4Dy	I4/mmm	tI26	$Mn_{12}Th$	0.885		0.511	39

Al_7Mn_5Dy, Al_6Mn_6Dy and Al_8Mn_4Dy are the solid solution phases in the form of $(Al_xMn_{1-x})_{12}Dy$. AlMnDy is solid solution phase in the form of $(Al_{1-x}Mn_x)_2Dy$

3. Results and Discussions

Table 2 lists the experimental results obtained from XRD and SEM/EDS analysis of 22 alloy buttons, as well as EPMA measurements on selected alloys.

A phase with nearly constant Dy (about 6-10 at.%) and various Mn/Al ratios was observed in alloys 7-22, as shown in Table 2. Some peaks of the x-ray pattern in these alloys are a match to $Mn_{12}Dy$, with slightly different lattice parameters. It was concluded that a solid solution, corresponding to $(Al_xMn_{1-x})_{12}Dy$, formed by Al substituting for Mn in $Mn_{12}Dy$ in this system. The maximum solid solubility of Al in $Mn_{12}Dy$ is 79.3 at.%, which is the average of alloys 20 and 21.

Note that both Al_2Dy and Mn_2Dy have the same cubic Cu_2Mg-type crystal structure. Similarly, phases with constant Dy content (about 30-33 at.%) and different Al/Mn ratio were observed in alloys 1-9,15-16 and 22, as listed in Table 2. The x-ray diffraction patterns of these phases were indexed by Al_2Dy or Mn_2Dy with slightly different lattice parameters. Thus it was concluded that, Al_2Dy and Mn_2Dy form a continuous solid solution, $(Al_{1-x}Mn_x)_2Dy$, in all these alloys.

Figure 1 is the backscattered electron (BSE) image and x-ray diffraction pattern of alloy 14. The light gray phase is $(Al_xMn_{1-x})_{12}Dy$, and the gray phase is Al_8Mn_5, while the dark needle phase is $Al_{11}Mn_4$. These three phases were identified by x-ray diffraction. Identification of phases in alloy 14 showed that there is a tie-triangle of $[(Al_xMn_{1-x})_{12}Dy + Al_8Mn_5 + Al_{11}Mn_4]$ in this system.

The phases $(Al_xMn_{1-x})_{12}Dy$, $Al_{11}Mn_4$, and Al_4Mn were observed to co-exist in alloy 17, as shown in Fig. 2. The EDS analysis showed that the white gray phase is $(Al_xMn_{1-x})_{12}Dy$, and the gray phase is $Al_{11}Mn_4$, while the dark gray phase is Al_4Mn. The dark gray phase was identified as Al_4Mn from its lower Al content.

The co-existence of $(Al_xMn_{1-x})_{12}Dy$, Al_6Mn, and (Al) was found in alloy 19, as shown in Fig. 3. Compositions of the identified phases are listed in Table 2. X-ray diffraction and EPMA confirmed the results of SEM/EDS analysis.

Direct evidences to support the tie-triangles of $[(Al) + Al_3Dy + (Al_xMn_{1-x})_{12}Dy]$, $[Al_3Dy + (Al_{1-x}Mn_x)_2Dy + (Al_xMn_{1-x})_{12}Dy]$, and $[Mn_{23}Dy_6 + (Al_{1-x}Mn_x)_2Dy + (Al_xMn_{1-x})_{12}Dy]$ are shown in Fig. 4, 5 and 6.

According to the Al-Dy phase diagram,[12] Al_2Dy_3 is formed by the peritectic reaction

Table 2 Phase identification by using XRD, SEM/EDS and EPMA for the selected Al-Mn-Dy alloys

	Compositions (at.%)							Measured Compositions EDS (at.%)			Measured Compositions EPMA (at.%)		
	Nominal			Measured									
No.	Al	Mn	Dy	Al	Mn	Dy	Phase identified	Al	Mn	Dy	Al	Mn	Dy
1	50	10	40	52.42	8.8	38.8	$(Al_{1-x}Mn_x)_2Dy$	56.9	10.9	32.2	56.9	12.0	31.1
							AlDy	51.4	1.0	47.6	40.8	7.4	51.8
							$AlDy_2$	34.6	0.9	64.5	32.4	1.9	65.7
2	40	15	45	41.8	16.3	41.9	$(Al_{1-x}Mn_x)_2Dy$	47.6	20.3	32.1	45.4	22.6	32.0
							$AlDy_2$	36.7	0.6	62.8	34.3	1.0	64.7
3	35	12.5	52.5	36.98	13.0	50.0	$(Al_{1-x}Mn_x)_2Dy$	44.1	23.5	32.5			
							$AlDy_2$	34.9	1.2	63.8			
							(Dy)	13.9	2.0	84.0			
4	27.5	17.5	55	31.33	16.5	52.2	$(Al_{1-x}Mn_x)_2Dy$	33.4	33.1	33.5			
							$AlDy_2$	34.4	1.8	63.8			
							(Dy)	5.1	2.1	92.8			
5	10	25	65	13.6	25.8	60.6	$(Al_{1-x}Mn_x)_2Dy$	18.2	49.4	32.4			
							(Dy)	4.9	1.5	93.6			
							$AlDy_2$	30.1	3.3	66.5			
6	15	40	45	18.55	36.8	44.7	$(Al_{1-x}Mn_x)_2Dy$	21.3	46.3	32.4	18.7	47.4	33.9
							(Dy)	3.2	2.8	94.0	0.1	0.1	99.8
							$AlDy_2$	26.4	5.7	67.9	28.4	2.7	68.9
7	17.5	60	22.5	23.63	47.6	28.8	$(Al_xMn_{1-x})_{12}Dy$	11.3	80.6	8.0	11.0	82.3	6.7
							$(Al_{1-x}Mn_x)_2Dy$	29.9	39.0	31.1	29.3	38.4	32.3
8	32.5	47.5	20	33.17	44.5	22.4	$(Al_xMn_{1-x})_{12}Dy$	33.1	58.3	8.6			
							$(Al_{1-x}Mn_x)_2Dy$	46.5	22.5	31.0			
9	20	67.5	12.5	13.65	69.1	17.3	$(Al_{1-x}Mn_x)_2Dy$	22.7	47.4	29.9	21.6	46.7	31.7
							$(Al_xMn_{1-x})_{12}Dy$	11.4	80.6	8.1	20.7	72.7	6.6
							$Mn_{23}Dy_6$	10.7	70.9	18.4	8.4	70.0	21.6
10	15	80	5	14.81	82.0	3.2	(βMn)	12.7	87.3	0.0	11.7	87.2	1.1
							$(Al_xMn_{1-x})_{12}Dy$	15.7	77.6	6.7	23.5	68.8	7.7
11	37.5	60	2.5	34.66	64.1	1.3	(βMn)	32.0	68.0	0.0	33.0	65.3	1.7
							$(Al_xMn_{1-x})_{12}Dy$	40.4	53.5	6.1	36.3	55.1	8.6
12	47.5	42.5	10	48.82	42.2	9.0	$(Al_xMn_{1-x})_{12}Dy$	51.0	41.7	7.3	52.4	38.8	8.8
13	55	35	10	55.79	35.4	8.8	$(Al_xMn_{1-x})_{12}Dy$	56.6	36.6	6.8	52.9	39.3	7.8
14	65	32.5	2.5	68.94	29.4	1.7	$(Al_xMn_{1-x})_{12}Dy$	63.8	30.0	6.2	62.1	28.7	9.2
							Al_8Mn_5	62.9	37.1	0.0	61.5	36.2	2.3
							$Al_{11}Mn_4$	72.8	27.2	0.0	72.5	24.4	3.1
15	50	27.5	22.5	53.71	25.4	20.9	$(Al_{1-x}Mn_x)_2Dy$	58.6	10.9	30.5	58.0	12.9	29.1
							$(Al_xMn_{1-x})_{12}Dy$	48.9	41.0	10.1	47.6	43.8	8.6
16	62.5	17.5	20	65.06	16.6	18.4	$(Al_{1-x}Mn_x)_2Dy$	63.1	3.9	33.0	63.5	3.5	33.0
							$(Al_xMn_{1-x})_{12}Dy$	64.9	28.4	6.8	62.7	27.8	9.5
							Al_3Dy	72.1	4.8	23.1	68.5	4.5	27.0
17	72.5	25	2.5	73.76	24.3	2.0	Al_4Mn	81.8	18.2	0	81.0	18.7	0.3
							$(Al_xMn_{1-x})_{12}Dy$	71.1	22.5	6.5	66.3	24.8	8.9
							$Al_{11}Mn_4$	75.7	24.1	0.2	73.2	24.9	1.9
18	72.5	15	12.5	74.45	13.8	11.7	Al_3Dy	76.1	0.9	23.0	73.4	1.7	24.9
							$(Al_xMn_{1-x})_{12}Dy$	74.5	19.4	6.1	69.3	21.8	8.9
19	82.5	12.5	5	88.09	8.8	3.2	$(Al_xMn_{1-x})_{12}Dy$	75.0	18.6	6.4	71.6	19.9	8.5
							(Al)	99.7	0.3	0.05	99.5	0.3	0.2
							Al_6Mn	85.9	14.1	0.0	84.7	13.7	1.6
20	85	7.5	7.5	89.45	5.6	5.0	Al_3Dy	77.2	0.6	22.2	75.5	0.5	24.0
							$(Al_xMn_{1-x})_{12}Dy$	76.3	17.0	6.7	74.1	17.2	8.7

Table 2 continued

No.	Compositions (at.%) Nominal Al	Mn	Dy	Measured Al	Mn	Dy	Phase identified	Measured Compositions EDS (at.%) Al	Mn	Dy	Measured Compositions EPMA (at.%) Al	Mn	Dy
							(Al)	99.6	0.3	0.1	99.6	0.1	0.3
21	92.5	2.5	5	96.04	1.3	2.7	$(Al_xMn_{1-x})_{12}Dy$	82.3	8.6	9.1	81.4	10.7	7.9
							Al_3Dy	77.4	0.2	22.4	78.4	0.4	21.2
							(Al)	99.5	0.2	0.3	99.7	0.2	0.1
22	60	10	30	64.85	8.4	26.7	$(Al_{1-x}Mn_x)_2Dy$	65.4	4.1	30.6	65.5	3.9	30.6
							$(Al_xMn_{1-x})_{12}Dy$	59.3	33.0	7.7	61.0	31.2	7.8

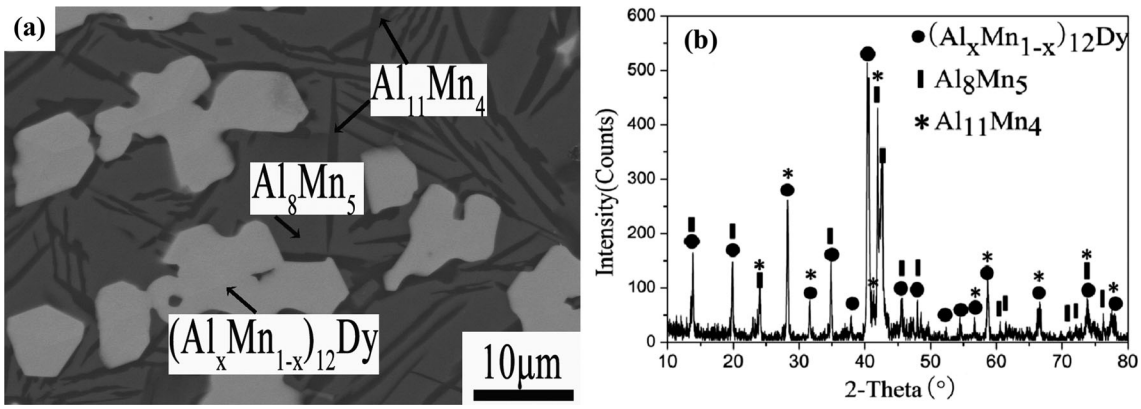

Fig. 1 (a) BSE image of the microstructure and (b) XRD results of alloy 14 annealed at 500 °C for 30 days

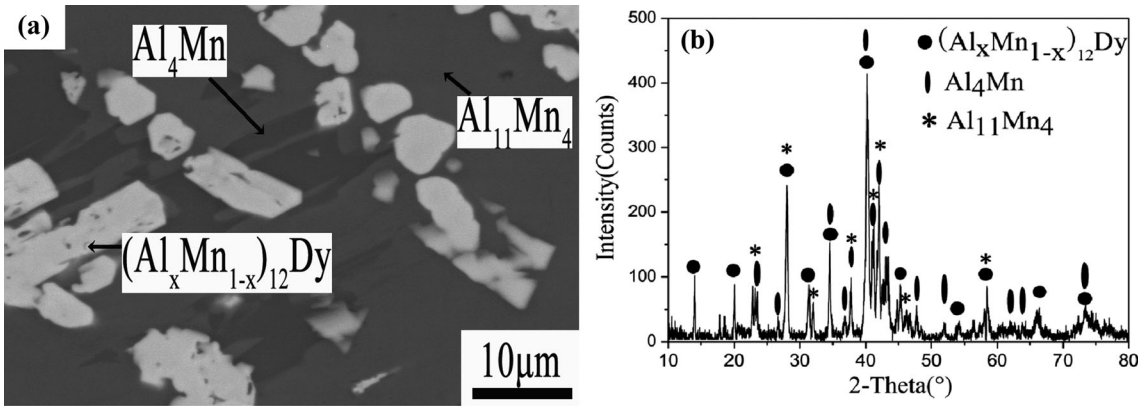

Fig. 2 (a) BSE image of the microstructure and (b) XRD results of alloy 17 annealed at 500 °C for 30 days

AlDy + Liquid → Al_2Dy_3, but Al_2Dy_3 was not observed in the current work. It is most likely that the phase does not form during rapid cooling following melting. Although AlDy and $AlDy_2$ will not co-exist when the alloy is in equilibrium, the co-existence of AlDy, $AlDy_2$ and $(Al_{1-x}Mn_x)_2Dy$ is observed in alloy 1, as shown in Table 2. That means that alloy 1 is off-equilibrium.

Phases with ~64 at.% Dy in alloys 1-6 were proven by XRD to be $AlDy_2$ rather than Al_2Dy_3. The crystal structure of Al_2Dy_3 was determined before in Ref 26 and 27. The Al_2Gd_3 type compounds Al_2Ho_3 and Al_2Er_3 form in the Al-Ho and Al-Er systems,[26,40] respectively. These are examples of the similarity between heavy RE metal compounds. Also, Al_2Dy_3 was observed in the determination of the Al-Mo-Dy ternary phase diagram at 600 °C.[5] Finally, Al_2Dy_3 appears stable below 600 °C according to the Al-Dy phase diagram in Ref 12. Thus, it is concluded that Al_2Dy_3 is stable at 500 °C.

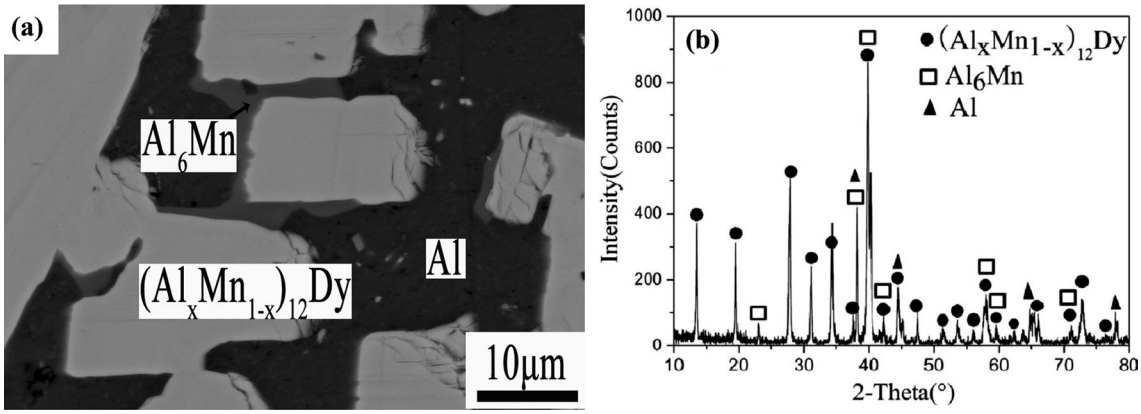

Fig. 3 (a) BSE image of the microstructure and (b) XRD results of alloy 19 annealed at 500 °C for 30 days

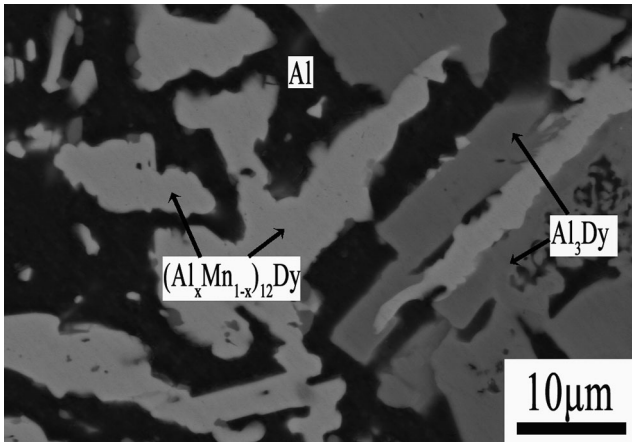

Fig. 4 BSE image of the microstructure of alloy 21, the dark phase is Al, the phase grey with point dispersed is Al_3Dy, the light gray phase is $(Al_xMn_{1-x})_{12}Dy$

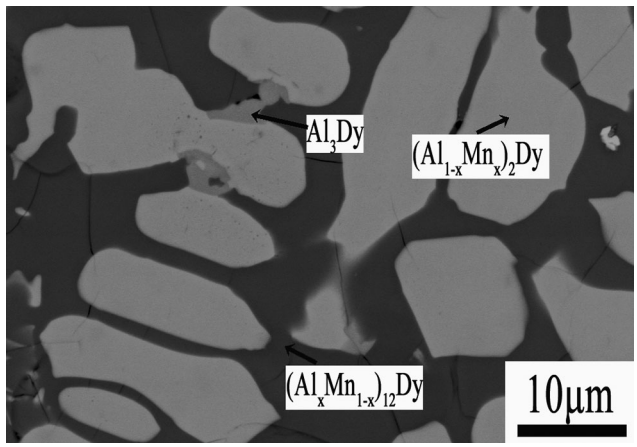

Fig. 5 BSE image of the microstructure of alloy 16, the gray phase is Al_3Dy, the light gray phase is $(Al_{1-x}Mn_x)_2Dy$, and the dark gray matrix phase is $(Al_xMn_{1-x})_{12}Dy$

The similar compound, Al_2Ho_3, forms by the peritectic reaction AlHo + liquid → Al_2Ho_3 at 994 °C.[41] Also, Al_2Ho_3 was confirmed to exist at 500 °C in the Al-V-Ho system.[42] The Al-V-Ho alloys were heated at 900 °C for 20 days to guarantee homogeneity before the 500 °C final heat treatment. The temperature of 900 °C was high enough for diffusion to enable the formation of Al_2Ho_3. In this work, alloys were kept at 500 °C and had no high temperature anneal. Apparently 500 °C is too low for sufficient diffusion to occur. Therefore it is assumed that Al_2Dy_3 is a stable phase at 500 °C and should be included in Fig. 7, although it was absent in the current work.

In the Al-Dy system,[12] the solubility of Al in (Dy) is negligible. A large amount of Al was detected in (Dy) in alloys 3, which shows that this alloy is off-equilibrium. Contents of Al in (Dy) in alloys 4-6 are smaller than that in alloy 3, which suggests that these alloys are closer to equilibrium.

Based on data available in Table 2, the phase diagram of the Al-Mn-Dy system was drawn, as shown in Fig. 7. It should be noted that the tie-triangles with solid lines are directly supported by the equilibrated alloys, and those with dash lines were deduced from the surrounding phase relationships.

The maximum solubility of Mn in Al_3Dy is 4.8 at.%, which was observed in alloy 16. Thus, the composition at the Al_3Dy corner of the tie-triangle $[Al_3Dy + (Al_{1-x}Mn_x)_2Dy + (Al_xMn_{1-x})_{12}Dy]$ is 72.1 at.% Al, 4.8 at.% Mn and 23.1 at.% Dy.

The maximum solubility of Mn in $AlDy_2$ is 5.7 at.%, which was observed in alloy 6. Thus the composition of the $AlDy_2$ corner in the tie-triangle $[AlDy_2 + (Al_{1-x}Mn_x)_2Dy + (Dy)]$ is 26.4 at.% Al, 5.7 at.% Mn and 67.9 at.% Dy.

The maximum solubility of Al in $Mn_{23}Dy_6$ is 10.7 at.%, which was observed in alloy 9. Thus the composition of the $Mn_{23}Dy_6$ corner of the tie-triangle $[Mn_{23}Dy_6 + (Al_{1-x}Mn_x)_2Dy + (Al_xMn_{1-x})_{12}Dy]$ is 10.7 at.% Al, 70.9 at.% Mn and 18.4 at.% Dy.

For the Al-rich alloy, the annealing temperature of 500 °C seems high enough for sufficient Al diffusion to

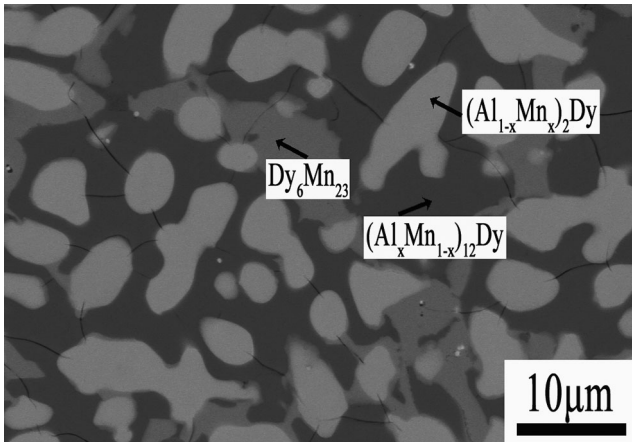

Fig. 6 BSE image of the microstructure of alloy 9, the gray phase is $Mn_{23}Dy_6$, the light gray phase is $(Al_{1-x}Mn_x)_2Dy$, and the matrix phase is $(Al_xMn_{1-x})_{12}Dy$

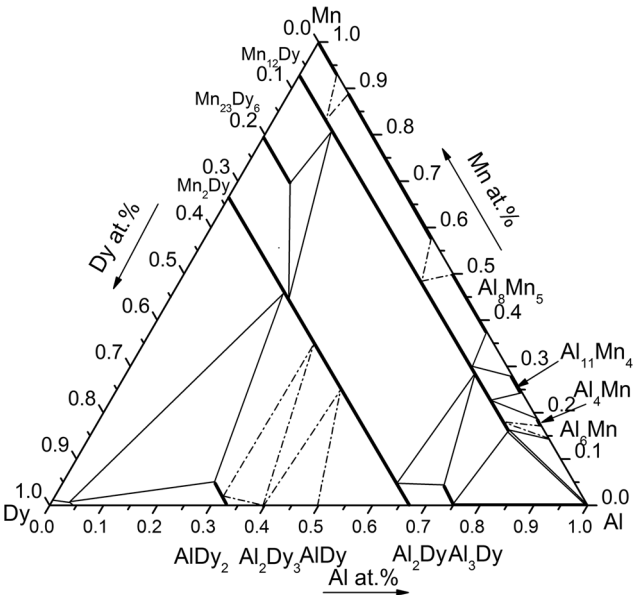

Fig. 7 The phase diagram of the Al-Mn-Dy system at 500 °C

achieve equilibrium, since the Al melting point is only 660 °C. The phase boundary in alloy 19 (Fig. 3) is very clear suggesting equilibrium. Results from alloy 19 are consistent with the previous experimental investigation of the Al-Mn phase diagram,[14, 15, 43, 44] which show that only Al_6Mn exists in the Al-rich corner at 500 °C, and disagrees with the thermodynamic description of the Al-Mn system.[45–47]

In addition, Gordillo et al.[6] studied the effect of heat treatment on an Al-5Mn-2Ce (at.%) alloy by using x-ray diffraction and electron microscopy. The master alloy was prepared by powder processing and extruding. The extrudate contained a mixture of fcc Al, $Al_{20}Mn_2Ce$, Al_6Mn and a small amount of $Al_{12}Mn$ and $Al_{11}Ce_3$. After heat treatment at 450 °C for 48 h, the $Al_{20}Mn_2Ce$ and Al_6Mn phases decomposed completely and the volume fraction of $Al_{12}Mn$ increased to 72-73 vol.%. Heat treatment at 500 °C for 48 h resulted in the decrease of $Al_{12}Mn$ volume fraction to 9 vol.%, while amounts of each phase in the Al-5Mn-2Ce alloy becomes 60 vol.% fcc Al, 22 vol.% $Al_3(Mn,Ce)$, 8 vol.% Al_6Mn and 1 vol.% $Al_{11}Ce_3$. After prolonged annealing for 30 days in our work, the $Al_{12}Mn$ phase was not observed. These results suggest that $Al_{12}Mn$ is metastable at 500 °C, and that the temperature of the peritectoid reaction $Al + Al_6Mn \rightarrow Al_{12}Mn$ is below 500 °C. That is lower than the reaction temperature of 507 °C predicted in the assessment work of Jansson.[45] Thus, $Al_{12}Mn$ is not included in the Al-rich corner in Fig. 7. In addition, it is hard to distinguished λ-Al_4Mn from μ-Al_4Mn. Therefore these two phases are treated as single Al_4Mn in this work.

4. Summary

1. The ternary phase equilibria relationships in the Al-Mn-Dy system at 500 °C have been established by XRD, SEM/EDS combining with EPMA techniques and deduced from the surrounding phase relationships. There are 12 tie-triangles in this system, of which five were measured and seven were deduced.
2. Two extensive solid solutions were found in this system. One was a continuous solid solution between Al_2Dy and Mn_2Dy to form $(Al_{1-x}Mn_x)_2Dy$. In the other solid solution, Al substitutes for Mn in $Mn_{12}Dy$ to form $(Al_xMn_{1-x})_{12}Dy$. The maximum solubility of Al in $Mn_{12}Dy$ is 79.3 at.%.
3. Al_2Dy_3 was not observed in the current work, which is assumed to be caused by difficulty forming Al_2Dy_3 both by the peritectic reaction $AlDy + Liquid \rightarrow Al_2Dy_3$ on cooling and by heat treatment at 500 °C.

Acknowledgments

This work was jointly supported by Guangxi Natural Science Foundation (No. 2013GXNSFAA019315), Guangxi Educational Institute Science Project (YB2014108), Guangxi Undergraduate Student Innovation project (2013CX061), and Science Project of Guangxi University for Nationalities (2011MDYB039).

References

1. Y. Du, S. Liu, L. Zhang, H. Xu, D. Zhao, A. Wang, and L. Zhou, An overview on phase equilibria and thermodynamic modeling in multicomponent Al alloys: focusing on the Al-Cu-Fe-Mg-Mn-Ni-Si-Zn system, *Calphad*, 2011, **35**(3), p 427-445
2. M.E. Krug, A. Werber, D.C. Dunand, and D.N. Seidman, Core-shell nanoscale precipitates in Al-0.06 at.% Sc microal-

loyed with Tb, Ho, Tm or Lu, *Acta Mater.*, 2010, **58**(1), p 134-145
3. Y. Harada and D.C. Dunand, Microstructure of Al_3Sc with ternary rare-earth additions, *Intermetallics*, 2009, **17**(1-2), p 17-24
4. S. Takayama and N. Tsutsui, A1-Sm and A1-Dy alloy thin films with low resistivity and high thermal stability for microelectronic conductor lines, *Thin Solid Films*, 1996, **289**(1-2), p 289-294
5. H. Wang, Y. Zhan, and W. Zhou, Phase equilibria of the Al-Mo-Dy ternary system at 873 K, *J Phase Equilib Diff*, 2013, **34**(4), p 322-327
6. M.A. Gordillo, I. Cernatescu, T.T. Aindow, T.J. Watson, and M. Aindow, Phase stability in a powder-processed Al-Mn-Ce alloy, *J. Mater. Sci.*, 2014, **49**(10), p 3742-3754
7. K.A. Darling, A.J. Roberts, L. Armstrong, D. Kapoor, M.A. Tschopp, L.J. Kecskes, and S.N. Mathaudhu, Influence of Mn solute content on grain size reduction and improved strength in mechanically alloyed Al-Mn alloys, *Mater. Sci. Eng. A*, 2014, **589**, p 57-65
8. D.X. Yang, X.Y. Li, D.Y. He, and H. Huang, Effect of minor Er and Zr on microstructure and mechanical properties of Al-Mg-Mn alloy (5083) welded joints, *Mater. Sci. Eng. A*, 2013, **561**, p 226-231
9. H. Li, J. Bin, J. Liu, Z. Gao, and X. Lu, Precipitation evolution and coarsening resistance at 400 °C of Al microalloyed with Zr and Er, *Scr. Mater.*, 2012, **67**(1), p 73-76
10. M.E. van Dalen, T. Gyger, D.C. Dunand, and D.N. Seidman, Effects of Yb and Zr microalloying additions on the microstructure and mechanical properties of dilute Al-Sc alloys, *Acta Mater.*, 2011, **59**(20), p 7615-7626
11. M.E. Van Dalen, D.C. Dunand, and D.N. Seidman, Microstructural evolution and creep properties of precipitation-strengthened Al-0.06Sc-0.02Gd and Al-0.06Sc-0.02Yb (at.%) alloys, *Acta Mater.*, 2011, **59**(13), p 5224-5237
12. H. Okamoto, Supplemental literature review of binary phase diagrams: Al-Bi, Al-Dy, Al-Gd, Al-Tb, C-Mn, Co-Ga, Cr-Hf, Cr-Na, Er-H, Er-Zr, H-Zr, and Ni-Pb, *J. Phase Equilib. Diff.*, 2014, **35**(3), p 343-354
13. J. Kim, M. Paliwal, S. Zhou, H. Choi, and I.-H. Jung, Critical systematic evaluation and thermodynamic optimization of the Mn-RE system (RE=Tb, Dy, Ho, Er, Tm and Lu) with key experiments for the Mn-Dy system, *J. Phase Equilib. Diff.*, 2014, **35**(6), p 670-694
14. H. Okamoto, Comment on Al-Mn (Aluminum-Manganese), *J. Phase Equilib.*, 1994, **15**(1), p 123-124
15. A.J. McAlister and J.L. Murray, The (Al-Mn) aluminum-manganese system, *J. Phase Equilib.*, 1987, **8**(5), p 438-537
16. J. Bandyopadhyay and K.P. Gupta, Low temperature lattice parameters of Al and Al-Zn alloys and Grüneisen parameter of Al, *Cryogenics*, 1978, **18**(1), p 54-55
17. G.D. Preston, The crystal structure of beta-manganese, *Philos. Mag.*, 1928, **5**(10), p 1207-1225
18. A.J. Bradley and J. Thewlis, The crystal structure of alpha-manganese, *Proc. R. Soc. Lond. Ser. A*, 1927, **115**(771), p 456-471
19. A. Nakaue, Studies on the pressure-temperature phase diagram of Nd, Sm, Gd and Dy, *J. Less. Common. Met.*, 1978, **60**(1), p 47-58
20. J.H.N.V. Vucht and K.H.J. Buschow, On the binary aluminium-rich compounds of the rare-earth elements, *Philips Res. Rep.*, 1964, **19**, p 319-322
21. N.C. Baenziger and J.J. Hegenbarth, Gadolinium and dysprosium intermetallic phases. III. The structures of Gd_3Al_2, Dy_3Al_2, Gd_5Ge_3, Dy_5Ge_3 and $DyAl_3$, *Acta Crystallogr.*, 1964, **17**(5), p 620-621
22. J.F. Cannon and H.T. Hall, Effect of high pressure on the crystal structures of lanthanide trialuminides, *J. Less Common. Met.*, 1975, **40**(3), p 313-328
23. M.M. Abd-el-Aal, A.S. Ilyushin, A.V. Pechennikov, Y.R. Sharapov, and V.I. Chechnerkov, The structure and magnetic properties of compounds of the $Dy_{1-x}Gd_xAl_2$ system, *Moscow Univ. Phys. Bull.*, 1987, **42**(3), p 126-129
24. N.C. Baenziger and J.L. Moriarty, Gadolinium and dyprosium intermetallic phases. II. Laves phases and other structure types, *Acta Crystallogr.*, 1961, **14**(9), p 948-950
25. C. Bècle and R. Lemaire, Structures cristallines des composés DyAl et CeAl et des autres composés equiatomiques de l'aluminium avec les métaux des terres rares, *Acta Crystallogr.*, 1967, **23**(5), p 840-845
26. K.H.J. Buschow, Rare earth-aluminium intermetallic compounds of the form RAl and R_3Al_2, *J. Less. Common Met.*, 1965, **8**(3), p 209-212
27. Y.R. Sharapov, A.S. Ilyushin, R.S. Torchinova, V.I. Chechernikov, and A.V. Pechennikov, Structure and magnetic Properties of The compound Dy_3Al_2 crystallized in conditions of Microgravitation, *Russ. Metall.*, 1988, **1988**(1), p 192-193
28. K.H.J. Buschow and A.S.V.D. Goot, The crystal structure of rare-earth aluminium compounds R_2Al, *J. Less. Common. Met.*, 1971, **24**(1), p 117-120
29. F.E. Wang and J.V. Gilfrich, The crystal structures of $LuMn_5$ and the RMn_{12} compounds (where R=Gd, Tb, Dy, Ho, Er and Tm), *Acta Crystallogr.*, 1966, **21**(4), p 476-481
30. H.R. Kiechmayr, Structures of rare earth metal-manganese compounds, *Z. Kristallogr.*, 1967, **124**(1), p 152-160
31. J.H. Wernick, S.E. Haszko, and D. Dorsi, Pseudo-binary systems involving rare earth laves phases, *J. Phys. Chem. Solids*, 1962, **23**(6), p 567-572
32. J.G. Barlock and L.F. Mondolfo, Structure of some aluminium-lron-magnesium-manganese-silicon alloys, *Z. Metallkd.*, 1975, **66**, p 605-611
33. A.D.I. Nicol, The structure of $MnAl_6$, *Acta Crystallogr.*, 1953, **6**(3), p 285-293
34. A. Kontio and P. Coppens, New study of the structure of $MnAl_6$, *Acta Crystallogr. Sect. B*, 1981, **37**(2), p 433-435
35. T. Onishi and Y. Nakatani, Crystal structures of $MnAl_6$ and $MnAl_4$, *J. Jpn. Inst. Light Met.*, 1975, **25**(7), p 253-258
36. C.B. Shoemaker, D.A. Keszler, and D.P. Shoemaker, Structure of μ-$MnAl_4$ with composition close to that of quasicrystal phases, *Acta Crystallogr. Sect. B*, 1989, **45**(1), p 13-20
37. A. Kontio, E.D. Stevens, P. Coppens, R.D. Brown, A.E. Dwight, and J.M. Williams, New investigation of the structure of Mn_4Al_{11}, *Acta Crystallogr. Sect. B*, 1980, **36**(2), p 435-436
38. K. Schubert, S. Bhan, W. Burkhardt, R. Gohle, H.G. Meissner, M. Pötzschke, and E. Stolz, Some structural results of metallic phases, *Sci. Nat.*, 1960, **47**(13), p 303
39. O. Moze, R.M. Ibberson, R. Caciuffo, and K.H.J. Buschow, On the preferential site occupation of T = Cr or Mn in rare earth compounds of the type RT_4Al_8, *J. Less Common Met.*, 1990, **166**(2), p 329-334
40. R.L. Davis, R.K. Day, J.B. Dynlop, and B. Barbara, Structure (Neutron) of Er_3Al_2, *Acta Crystallogr. Sect. C*, 1987, **43**, p 1675-1677
41. K.A. Gschneidner, Jr., and F.W. Calderwood, Al-Ho(Aluminium-Holmium), *Binary alloy phase diagrams*, Vol 1, II, ed., T.B. Massalski, Ed., American Society for Metals, Metals Park, 1990, p 160-161
42. Y. Zhan, Z. Yang, H. Mo, and Y. Du, Phase equilibria of the Al-V-RE (RE=Gd, Ho) Systems at 773 K (500 °C), *Metall. Mater. Trans. A*, 2011, **43**(1), p 29-36

43. T. Gödecke and W. Köster, An addition to the phase diagram of the Al-Mn system, *Z. Metallkd.*, 1971, **62**, p 727-732
44. Z.A. Sviderskaya, E.S. Kadaner, N.I. Turkina, and V.I. Kuzmina, Boundary of the solid solution in the aluminum corner of the Alumimun-Mangnaese-Lithium system, *Met. Sci. Heat Treat.*, 1963, **5**(12), p 684-687
45. A. Jansson, A thermodynamic evaluation of the Al-Mn system, *Metall. Mater. Trans. A*, 1992, **23**(11), p 2953-2962
46. X.J. Liu, I. Ohnuma, R. Kainuma, and K. Ishida, Thermodynamic assessment of the aluminum-manganese (Al-Mn) binary phase diagram, *J. Phase Equilib.*, 1999, **20**(1), p 45-56
47. Y. Du, J. Wang, J.R. Zhao, J.C. Schuster, F. Weitzer, R. Schmid-Fetzer, M. Ohno, H.H. Xu, Z.K. Liu, S.L. Shang, and W.Q. Zhang, Reassessment of the Al-Mn system and a thermodynamic description of the Al-Mg-Mn system, *Z. Metallkd.*, 2007, **98**(9), p 855-871